Toxicology Letters 355 (2022) 19–30

Contents lists available at ScienceDirect

Toxicology Letters

journal homepage: www.elsevier.com/locate/toxlet

Investigating the interaction between organic anion transporter 1 and ochratoxin A: An *in silico* structural study to depict early molecular events of substrate recruitment and the impact of single point mutations

Jochem Louisse[a], Jean Lou C.M Dorne[b], Luca Dellafiora[c,*]

[a] Wageningen Food Safety Research, P.O. Box 230, 6700 AE, Wageningen, the Netherlands
[b] Scientific Committee and Emerging Risks Unit, European Food Safety Authority, Via Carlo Magno 1A, Parma, 43124, Italy
[c] Department of Food and Drug, University of Parma, Parma, 43124, Italy

HIGHLIGHTS

- Organic anion transporters (OATs) are important to regulate xenobiotics disposition.
- OATs are poorly characterized from a mechanistic point of view.
- The OAT1-dependent transport of ochratoxin A has been investigated.
- Mechanics of OATs involved in substrates recruitment have been described.
- A mutation possibly preventing ochratoxin A recruitment has been identified.

ARTICLE INFO

Article history:
Received 14 June 2021
Received in revised form 18 October 2021
Accepted 2 November 2021
Editor: Dr. Angela Mally
Available online 5 November 2021

Keywords:
Organic anion transporter 1
Ochratoxin A
3D molecular modelling
Toxicokinetics
Human risk assessment

ABSTRACT

Organic anion transporters (OATs) belong to a subgroup of the solute carrier 22 transporter family. OATs have a central role in xenobiotic disposition affecting the toxicokinetics of its substrates and inter-individual differences in their expression, activity and function impact both toxicokinetics and toxicodynamics. Amongst OATs, OAT1 (solute carrier family 22 member 6) is involved in the urinary excretion of many xenobiotics bringing substrates into renal proximal tubular cells which can then be secreted across the apical membrane into the tubule lumen. The mycotoxin ochratoxin A has been shown to have a high affinity for OAT1, which is an important renal transporter involved in its urinary excretion. Nowadays, molecular modeling techniques are widely applied to assess protein-ligand interactions and may provide a tool to depict the mechanic of xenobiotic action be it toxicokinetics or toxicodynamics. This work provides a structured pipeline consisting of docking and molecular dynamic simulations to study OAT1-ligand interactions and the impact of OAT1 polymorphisms on such interactions. Such a computational structure-based analytical framework allowed to: i) model OAT1-substrate complex formation and depict the features correlating its sequence, structure and its capability to recruit substrates; and ii) investigate the impact of OAT1 missense mutations on substrate recruitment. Perspectives on applying such a structured pipeline to xenobiotic-metabolising enzymes are discussed.

1. Introduction

Organic anion transporters (OATs) belong to a subgroup of the solute carrier 22 (SLC22) transporter family that have a ubiquitous distribution in animal species including expression in a wide range of tissues such as kidney, liver, brain, placenta, retina, and olfactory mucosa (Nigam et al., 2015). OATs play an important role in the regulation of trans-membrane and trans-cellular transport of endogenous low-molecular weight molecules, such as hormones and other signaling molecules, and a wealth of xenobiotics such as natural toxins, drugs, and food constituents (Lai et al., 2018). In this context, OATs have a central role in xenobiotic disposition affecting

* Corresponding author.
E-mail address: luca.dellafiora@unipr.it (L. Dellafiora).

http://dx.doi.org/10.1016/j.toxlet.2021.11.001

absorption, distribution, metabolism, and excretion (ADME) of OAT substrates and inter-individual differences in expression, activity and function of OATs impact both their toxicokinetics (TK) and toxicodynamics (TD) (Zhang et al., 2021).

With regards to the elimination of pharmacologically active compounds and toxicants, the kidney is considered the central organ responsible for excretion. Substances can be excreted *via* passive excretion by filtration of the blood through the glomeruli, typically excreting the unbound fraction of chemical to the pre-urine, and by active transport processes from the kidney blood to the pre-urine *via* the renal proximal tubule cells. For the active transport, kidney proximal tubule cells express several transport proteins, including OATs, regulating the trafficking of molecules from the bloodstream to proximal tubule lumen, and vice versa, eventually determining the excretion of chemicals *via* urine (Sweet, 2005).

Further understanding of the relationships between molecular features of transporters and their functions (transport of substrates) provide important insights into their role in the elimination, internal exposure and the associated toxicity of food-related xenobiotics (Zhang et al., 2021). In this regard, the OAT family is poorly understood from a structural biology standpoint, as no crystallographic nor NMR structures have been depicted and made available so far. As a consequence, defining features that correlate OAT sequence, structure and their induced-fit movements to the capability to efficiently recruit and translocate substrates remains a challenge. Indeed, lack of a direct structural description and information on the architecture of substrate binding prevents a full understanding of the mechanisms underpinning the transport of substrates and the move towards kinetically informed chemical risk assessment for OAT substrates (Clerbaux et al., 2019). A clear understanding of mechanistic aspects behind OAT substrates recruitment and translocation would shed light on the inter- and intra-species differences in TK and related TD and would ultimately provide a mechanistic basis for more science-based risk assessments of OAT substrates.

Moreover, depicting OAT-substrate complex formation at the structural and molecular level would also allow to assess the impact of missense mutations of OATs on the TK of relevant compounds, including those causing lower renal clearance and related higher internal exposure. This would provide a valuable basis to identify human subpopulations with a particular susceptibility to such xenobiotics and allow to take into account such inter-individual differences in risk assessment. In this respect, polymorphisms of transporters have already been well documented, with some variants recurring in a number of cancers, and their effects on the TK of specific compounds have also been described (e.g. Buxhofer-Ausch et al., 2020; Rocha et al., 2018; Sissung et al., 2014; Wang et al., 2019).

Amongst transporters, OAT1 is directly involved in the excretion of a wealth of compounds *via* the urine as it brings substrates into renal proximal tubular cells where they can be secreted across the apical membrane into the tubule lumen (Fujita et al., 2005). OAT1 is mainly expressed in the kidney and is particularly localized in the basolateral membrane of proximal tubular cells (Saito, 2010). The mycotoxin ochratoxin A (OTA) has been well studied for its nephrotoxic and hepatotoxic effects and has been shown to have a high affinity for OAT1, considered as an important renal transporter involved in its urinary excretion (Anzai et al., 2010; Jung et al., 2001; Pickova et al., 2020). OTA is known for its relatively long half-life in a range of animal species, particularly in humans (Anzai et al., 2010; Ringot et al., 2006), and it may therefore accumulate upon repeated exposure. The long half-lives are related to a low rate of biotransformation, the high binding to serum proteins, especially to albumin, and related limited glomerular filtration, as well as to enterohepatic recirculation (Kimura et al., 2002; Williams et al., 2021; Zhang et al., 2021). Active tubular secretion is thought to be an important pathway of elimination, in which organic anion transporters (OATs) play a major role (Anzai et al., 2010; Ringot et al., 2006). It has been shown that OTA is a substrate for human OAT1, OAT3 and OAT4 (Babu et al., 2002; Jung et al., 2001; Tsuda et al., 1999), although OAT1 has the highest affinity, as per USCD-FDA TransPortal database (Morrissey et al., 2012). These transporters are involved in the tubular secretion (OAT1 and OAT3) and the reabsorption (OAT4) of small molecules. *in vitro* evidence has shown that OAT1 polymorphism (SLC22A6) influences the cellular uptake of OTA (Fujita et al., 2005), suggesting possible related inter-individual differences in OTA TK. OTA's relevance to the food safety area has been unambiguously ascertained (EFSA, 2020), but little evidence is available with regards to the possible impact of inter-individual differences in TK, including OAT1 polymorphisms, on the TD of OTA.

On the basis of the above, as a proof of principle, the present manuscript aimed at providing a computational structure-based analytical framework to: i) model the OAT1-substrate complex formation to underpin early features correlating the sequence and structure of OAT1 and its capability to recruit OTA and other substrates; and ii) estimate the effects of missense mutations of OAT1 on the very early mechanisms underpinning OTA recruitment. In other words, in line with the current proposals to apply new approach methodologies (NAMs) for human risk assessment (Williams et al., 2021), this work aimed at providing a prompt pipeline to investigate substrate recruitment with OAT1, including OTA and other compounds, and investigate the impact of OAT1 mutations on OTA's TK based on early recruitment mechanisms. To do so, a 3D molecular modeling study was applied. Such 3D molecular modeling techniques are nowadays widely used and accepted to investigate protein-ligand interactions and, in the case of OAT1, may provide a basis for mechanistic evaluation of either TK and TD aspects of its substrates (Ng and Hungerbuehler, 2015; Xu and Chen, 2020). In this context, a pipelined procedure consisting of docking studies and molecular dynamic simulations was applied to provide a reliable workflow to study the OAT1-ligand interaction and to investigate whether specific OAT1 polymorphisms may affect the early capability to recruit OTA with possible consequences on its TK and related toxicity. It is important to note that the aim of this study was to develop a pipeline that can be used to study early interactions with xenobiotics and OAT1 and provide mechanistic insights to better characterise their TK. OTA was selected as a model xenobiotic relevant to food safety in the present study, but the aim was not to provide a full mechanistic analysis of the overall TK of OTA or an in-depth analysis of system biophysics. For a more complete mechanistic insight with regards to the TK of OTA, one should also assess OTA interactions with other transporter proteins and biotransformation enzymes.

Overall, the structurally informed analytical approach presented here allows to provide mechanistic insights in OAT-substrate interactions to increase our understanding of the disposition of OAT substrates. In addition, this study provides evidence of the impact of mutations, occurring in certain cancers, which might alter OTA's TK and TD. Further studies are proposed to deepen the mechanistic understanding of OAT1's function and that of other transporters in the TK and TD of xenobiotics.

2. Material and methods

2.1. Data source

The set of low-molecular weight molecules analyzed in this work included OTA, 6-carboxyfluorescein, *para*-aminohippuric acid, prostaglandin E2, homostachydrine, glycitein-7-glucuronide,

pravastatin and beta-muricholate. The 3D structures were all retrieved in the 3D structure-data file (.sdf) format from the PubChem database (https://pubchem.ncbi.nlm.nih.gov) (Kim et al., 2021) with the following respective PubChem CID: 442530, 76806, 2148, 5280360, 45782894, 54670067, 54687 and 5283853. The primary sequence of human OAT1 (Solute carrier family 22 member 6) was retrieved in the FASTA format from the UniProt database (https://www.uniprot.org) (Bateman et al., 2021) with the code Q4U2R8. The availability of 3D structures of human OAT1 was checked in the Protein DataBank (PDB; https://www.rcsb.org) (Berman et al., 2000) but no entries were found (last database access: 5th of May 2021).

2.2. Homology modeling

Homology modeling was used to derive the 3D structure of human OAT1 as no structures were publicly available at the time of analysis (last access to PDB: 5th of May 2021). To do so, the trRosetta algorithm (https://yanglab.nankai.edu.cn/trRosetta) (Yang et al., 2020) was used with the human OAT1 sequence in the FASTA format as input and allowing the search of PDB templates for a better prediction. Briefly, trRosetta is an algorithm for a fast and accurate protein structure prediction. It builds the protein structure based on direct energy minimizations with a constrained optimization by Rosetta (Simons et al., 1999). The restraints include inter-residue distance and orientation distributions, predicted by a deep residual neural network. Homologous templates found in PDB were included in the network prediction to improve the accuracy of the predicted OAT1 3D structure. The manual search of homologous proteins in PDB was done using the sequence of OAT1 as input in the online blastp tool (https://blast.ncbi.nlm.nih.gov) (Altschul et al., 1997) to complement the information of templates automatically identified by trRosetta choosing the PSI-BLAST algorithm with 2 iterations and default parameters. Moreover, the multiple-sequence alignment (MSA) of OAT1 sequence and those of templates used by trRosetta to refine the model prediction was performed using Clustal X (version 2.1) (Larkin et al., 2007) setting gap opening penalty at 10 and gap extension penalty at 1, and choosing PAM series as protein weight matrix. The MSA was visualised and plotted using CLC Sequence Viewer 7.7 (https://digitalinsights.qiagen.com/).

2.3. Model and ligands preparation

The consistency of all atom and bond type assignment and geometries of ligands and the OAT1 model was visually checked with UCSF Chimera software (version 1.15) (Pettersen et al., 2004). Specifically, the correctness of ligands stereochemistry was cross-checked while comparing their 3D structure with the respective stereochemistry reported in the CAS SciFinder database (https://scifinder-n.cas.org), which is a multi-purpose "gold standard" benchmark database for small molecules. The CAS registry number for OTA, 6-carboxyfluorescein, *para*-aminohippuric acid, prostaglandin E2, homostachydrine, pravastatin and beta-muricholate were 303–47-9, 3301–79-9, 61–78-9, 363–24-6, 472–22-0, 81093–37-0 and 2393–59-1, respectively. In contrast, glycitein-7-glucuronide was not annoted in the CAS SciFinder^{n} database and its stereochemistry was checked with that of glycitein (CAS registry number 40957–83-3) and glucuronid acid (CAS registry number 6556–12-3). Mutated variants of OAT1 were derived replacing specific amino acid side-chains using the Structure Editing/Rotamer tool of UCSF Chimera software (version 1.15) (Pettersen et al., 2004) and choosing the rotamer with the highest computed probability to occur when multiple rotamers were computed. All the carboxylic groups of ligands were deprotonated as expected under physiological conditions and the 3D structures were saved as Tripos MOL2 molecule file (.mol2) for subsequent analysis. The OAT1 model was further relaxed and energetically minimized to avoid steric clashes and to correct on the all structures any eventual improper geometries by mean of GROMACS (Abraham et al., 2015) with CHARMM27 all-atom force field parameters support (Best et al., 2012). In particular, the steepest descent minimization algorithm was used with an energy step size of 0.01, a maximum allowed number of steps set at 5000 and an energy threshold to stop minimization set at 10.0 kJ/mol. This post-processing step was also applied to the mutated variants prior to perform the docking simulations to account for the possible local mutation-induced arrangements of the protein structure. Moreover, the stability of mutated OAT1 variants was calculated using the PremPS method (Chen et al., 2020). This method provides a specific and accurate assessment of the impact of missense mutations on protein stability through the implementation of a random forest regression scoring function to estimate unfolding Gibbs free energy changes ($\Delta\Delta G$).

The RMSD (root-mean squared deviation) values of the OAT1 model versus the template structures, used to refine the model, were calculated using a sequence-independent and whole-structure alignment using the Open-Source PyMOL software (http://www.pymol.org) with the "super" command. The alignment and RMSD calculation of transmembrane domains was performed with UCSF Chimera software (version 1.15) (Pettersen et al., 2004) instead using the MatchMaker tool (setting Smith-Waterman algorithm and BLOSUM-62 matrix).

2.4. Docking analysis

The docking analysis was done using the AutoDock Vina software (version 1.1.2) (Trott and Olson, 2010) graphically interfaced in the UCSF Chimera software (version 1.15) (Pettersen et al., 2004). The binding site has been defined within a box (35.64 $\times$ 33.99 $\times$ 23.75 L x W x H) centered at the channel entrance. Default parameters were used except for the number of binding modes that was set at 1, the exhaustiveness of research that was set at 4 and the maximum energy difference that was set at 3 kcal/Mol.

2.5. Molecular dynamic simulations

Molecular dynamic simulations were performed to investigate the overall geometrical stability of OAT1-ligand complexes over the time. Molecular dynamic simulations were performed using GROMACS (version 5.1.4) (Abraham et al., 2015) with CHARMM27 all-atom force field parameters support (Best et al., 2012). All the ligands have been processed and parameterized with CHARMM27 all-atom force field using the SwissParam tool (http://www.swissparam.ch) (Zoete et al., 2011). Input structures were solvated with SPCE waters in a cubic periodic boundary condition, and counter ions (Na^+ and Cl^-) were added to neutralize the system. The membrane and its effect on the maintenance of the overall protein folding was implicitly accounted for by setting position restraints to the protein's non-hydrogen atoms (type 1, with the x,y,z values set at 1000 each), to allow movement from the reference position with an energy penalty. Prior to performing molecular dynamic simulations, the systems were energetically minimized to avoid steric clashes and to correct improper geometries using the steepest descent algorithm with a maximum of 5000 steps. Afterwards, all the systems underwent isothermal (300 K, coupling time 2 psec) and isobaric (1 bar, coupling time 2 psec) 100 psec simulations before running an early-term 25 nsec simulation to monitor the earliest induced-fit movements (300 K with a coupling time of 0.1 psec and 1 bar with a coupling time of 2.0 psec).

3. Results and discussion

3.1. Reliability assessment and structural analysis of OAT1 model

The reliability of the OAT1 model was assessed using a three-tiered approach evaluating the consistency of its topological assignment first, then its geometrical consistency and finally its capability to discriminate substrates (i.e. ligands that are actually bound and transported) from decoys (i.e. molecules that are not bound or transported). The model was built from 2815 homologous sequences identified in the uniclust30_2018_08 database (Mirdita et al., 2017). Multiple sequence alignments are provided in the Supporting material. The model was then refined based on five homologous structures (PDB code 4ZW9, 6HD7, 5EQH, 5EQG and 5EQI) with well characterised structures that were automatically selected by trRosetta from the PDB70 database. Multiple sequence alignments are provided in Fig. 1S of the Supporting material.

In the first-tier assessment, the consistency of OAT1's topological assignment (reported in Fig. 2S of the Supporting material) was assessed on the basis of the TM-score (i.e., Template Modeling score), which is a numerical entity to predict the quality of full-length protein models (Yang et al., 2020; Zhang and Skolnick, 2004). The model recorded a TM-score above 0.5 pointing at a correct topological assignment, in agreement with previous studies (Yang et al., 2020).

In the second tier, the geometrical and topological consistency of the model was visually verified in the light of the little structural information available so far. In this respect, the model presented a 12-helices core, which is the protein region meant to be embedded into the cell membrane, and two domains corresponding to the extracellular and cytosolic region of OAT1, respectively. N- and C-terminus were both oriented toward the cytosolic region of the protein. Of note, as shown in Fig. 1, the calculated organization was in stark agreement with the 2D topology described for OAT1 which consist of 12 trans-membrane alpha helices with two major domains formed by the loops in between helices 1 and 2 (i.e. the large extracellular domain), and 6 and 7 (i.e. the small cytosolic domain) (El-Sheikh et al., 2008; Pelis and Wright, 2014). After assessing the consistency of topological assignment, the 3D structure of OAT1 was compared to those of homologous structures found in PDB. Although no OATs were found, the search of homologous structures in PDB highlighted the presence of several phylogenetically related trans-membrane transporters sharing the highly conserved 12-helices trans-membrane domain.

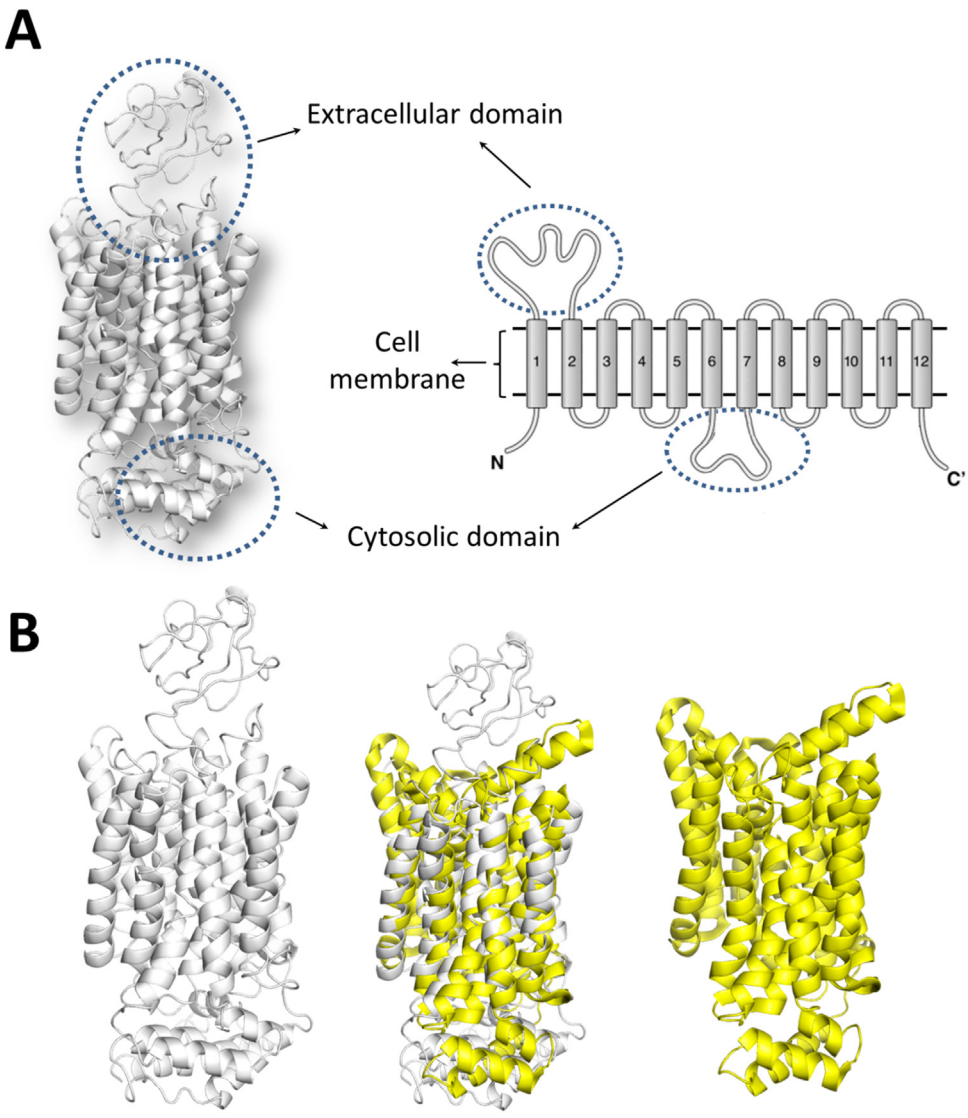

Fig. 1. Graphical representation of OAT1 model. **A.** 3D ribbon-tube and 2D representation of OAT1. **B.** 3D organization of OAT1 (white) in comparison to the crystallographic structure of GLUT1 (yellow; PDB code 4PYP).

The homolog sequence with the highest query coverage was the human glucose transporter GLUT1 in the inward conformation (PDB code 4PYP) (Deng et al., 2014). In this respect, the query coverage is represented by a percentage value which describes the coverage contribution of the query sequence compared to that in homologous sequences. A close analysis of the blastp alignment (Fig. 3S; Supporting material) revealed that the relatively low coverage was mostly due to the fact that GLUT1 structure missed the huge extracellular loop between helix 1 and helix 2 of OAT1. However, GLUT1 is a glucose uniporter responsible for constitutive or basal glucose uptake with a 12-helices trans-membrane domain (Deng et al., 2014; Kapoor et al., 2016). The structural alignment between the OAT1 model and this GLUT1 structure scored a RMSD value of 7.8 Å. As shown in Fig. 1B, the structural comparison between the OAT1 model and the crystallographic structure of GLUT1 revealed the conservation of the transmembrane core, confirmed the correctness of topological assignment and helices disposition, thereby further supporting the reliability of OAT1 model geometry. Furthermore, the primary and tertiary structure of the OAT1 model was also compared to that of the five templates selected by trRosetta to improve model accuracy. Supporting material provides multiple-sequence alignments. In this context, four protein structures were available for human glucose-transporters namely one for GLUT3 in the outward conformation and three for GLUT1 in the inward conformation with PDB code 4ZW9, 5EQG, 5EQH and 5EQI, respectively (Deng et al., 2014; Kapoor et al., 2016). The fifth protein structure available was a plant sugar transporter in the outward conformation having PDB code 6H7D (Paulsen et al., 2019). With regards to primary structures, these five homologues showed a sequence coverage above 71 % over the OAT1, with a sequence identity ranging between 21.8 and 23.4 % (Table 1S, Supporting Material). In contrast, all tertiary structures showed the same 12-helices trans-membrane core found in the OAT1 model further supporting the consistency of its topological assignment. With regards to the structure superimposition, OAT1 was more similar to the GLUT1 structures in the inward conformation (with RMSD values ranging from 7.5 to 7.7 Å) than to the other two transporters in the outward conformation (with RMSD values ranging from 8.0 to 8.3 Å). However, when looking at the 12-helices trans-membrane region only, the structure in the outward conformation (PDB code 4ZW9) recorded the lowest RMSD value (i.e. 1.2 Å) compared to 4PYP, 5EQG, 5EQH, 5EQI and 6HTD, with RMSD values of 1.4, 1.3, 1.3, 1.5 and 1.4 Å, respectively. Notably, assessing similarities in terms of organization at the level of transmembrane domain is more probative to hypothesise the transporter conformation than considering the RMSD of the overall structure. On this basis, the outward conformation of the OAT1 model was inferred. Of note, the RMSD analysis of crystallographic structures revealed relatively little differences between the inward and outward crystallographic conformations analysed here, with an average RMSD between the transmembrane region of the structure in the outward conformation and those in the inward conformation of 0.75 Å. This could suggest that pronounced structure reorganization takes place during the substrate translocation, while the transporter that is ready to receive a substrate might have an overall conformation closely related to that occurring after the substrate has been released within the cell. On this basis, our model could serve as a valid starting point to study the mechanics of early contacts between OAT1 and low-molecular weight molecules. Nonetheless, the crystallographic conditions might have reduced the differences between the two opposite transporter conformations, making further dedicated studies important to better understand the system mechanics.

The third tier of model evaluation consisted of the assessment whether the model was able to discriminate substrates from decoys using a structure-based molecular modeling approach relying on docking analysis and molecular dynamic simulations, as previously described (Dellafiora et al., 2015). In this respect, the capability of distinguishing the so defined “true ligands” (i.e. molecules experimentally demonstrated as substrates for the protein under analysis) from decoys (i.e. nonbinding compounds) is a well-recognised method to validate structure-based models (Graves et al., 2005). To do so, the solvent exposed extracellular surface of OAT1 was visually inspected to identify a reasonable region to dock ligands. As shown in Fig. 2, a surface cleft in between the trans-membrane core and the large extracellular domain between helix 1 and 2 can clearly be seen. A closer look at the inner part of this surface cleft revealed the presence of an arginine residue (Arg134) with the side chain well exposed to the solvent. The guanidinium group, which is expected to be positively charged under physiological conditions, adopted an orientation prone to interact with the anionic moiety of incoming substrates and might

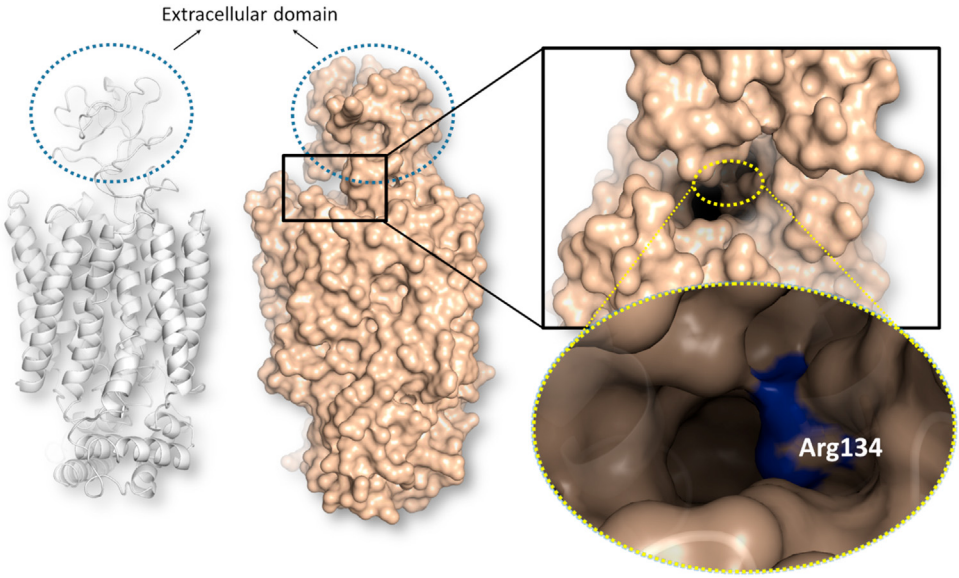

Fig. 2. Graphical representation of ligand binding site considered in docking studies. The protein is shown either in ribbon-tube or in surface representation. The close-ups detail the binding site and the position of Arg134 is colored in blue.

act as the very first molecular driving force to strive the passage of substrates through the transporter. Therefore, a docking study was run setting the ligand binding site there and choosing as OAT1 ligands a selection of the highest-affinity probe substrates listed in the USCD-FDA TransPortal database (Morrissey et al., 2012). The set of ligands included, along with OTA, 6-carboxyfluorescein, *para*-aminohippuric acid and prostaglandin E2 (Fig. 3). As reported in the USCD-FDA TransPortal database, all these ligands have been already described as high affinity substrates of OAT1 with K_m values in the low μM range (Cihlar and Ho, 2000; Islinger et al., 2001; Jung et al., 2001; Kimura et al., 2002). The set of decoys was collected from the scientific literature and included homostachydrine, glycitein-7-glucuronide, pravastatin and beta-muricholate (Fig. 3) as previous studies ascertained that they are not appreciably transported or bound by OAT1 (Bush et al., 2017; Takeda et al., 2004; Wong et al., 2011). Of note, the docking software used in this study used a scoring function that provides an estimate of the binding energy (i.e. the more negative the score, the more stable the expected stability of the protein-ligand complex). However, as shown in Table 2, the scoring function was not able to discriminate substrates from decoys, as all of them recorded scores plausibly supporting a certain capability to form a complex with OAT1. Nevertheless, the two classes of compounds had an appreciably diverse geometry of interaction. Indeed, as shown in Fig. 4, OTA and the other substrates sunk to a higher extent into the surface cleft compared to decoys. In particular, all the substrates, but none of the decoys considered here, placed the carboxylic group close and toward the guanidinium group of Arg134 (Fig. 4; Table 2) adopting a proper orientation to form polar interactions. These results were in agreement with the hypothesis that the presence of an inner positively charged spot into the surface cleft might have a role to drive the proper orientation and binding of substrates promoting their transfer. Of note, the results collected for decoys, and in particular the docking scores that could not exclude the existence of a certain degree of protein-decoy interaction, may suggest that a number of non-substrates might occasionally interact with OAT1, but with orientation and localisation that do not allow for efficient transport.

The interaction with OAT1 was then assessed for a selection of molecules (2 substrates and 2 decoys; OTA, *para*-aminohippuric acid, beta-muricolate and homostachydrine) by mean of molecular dynamic simulations. Molecular dynamic simulations served to: i) study the early induced-fit movements of OAT1, possibly relevant for the stability of protein-ligand complexes over the time; and ii) identify further mechanistic features, meant to be integrated to those derived from docking studies, to better discriminate substrates from decoys. In particular, the stability of complexes was studied from a geometrical standpoint monitoring ligands and protein trajectories along with the analysis of their root-mean-square deviation (RMSD). As shown in Fig. 5, the geometrical landscape of substrates was clearly different from that of decoys. In particular, although the protein RMSD was found similar in the four complexes, the ligands showed a different and intrinsically variable trend in terms of RMSD values, which suggested a discrete deviation from the starting position possibly indicating the existence of movement pathways over the OAT1 surface. Homostachydrine had the most stable trend along the all simulation suggesting the lack of appreciable movements. A closer look at the trajectory of the ligands revealed that OTA and *para*-aminohippuric acid drew an inward trajectory toward the transmembrane core of OAT1, reasonably preluding the trans-membrane transport. Conversely, homostachydrine was found stuck at the starting position along the all simulation, while beta-muricholate, which had the most different RMSD trend compared to the others, showed an outward trajectory leaving the surface cleft. In addition, OAT1 in complex with the two substrates OTA and *para*-aminohippuric acid underwent more discrete and relatively wider movements of the region surrounding the ligand binding site formed by part of helix 11 and 12 compared to those observed in the two complexes with decoys (Fig. 5C). Specifically, at the beginning of the simulation, the two complexes with substrates showed an early opening of such a region, which allowed the substrate entrance followed by a tendency to close again once the substrate has started its inward trajectory. This tendency might suggest the presence of movements that prelude the closure of the transporter over the entered ligands. Interestingly, these movements were not seen when OAT1 was in complex with decoys. Overall, these data could provide a mechanistic explanation to understand, at least in part, why the decoys considered in this study are not suitable for being transported by OAT1.

On the basis of the above, the capability to arrange the anionic portion close to the positively charged inner part of the surface cleft and the subsequent capacity to elicit an opening of the binding site promoting substrates entrance were identified as mechanistic features to discriminate substrates from decoys.

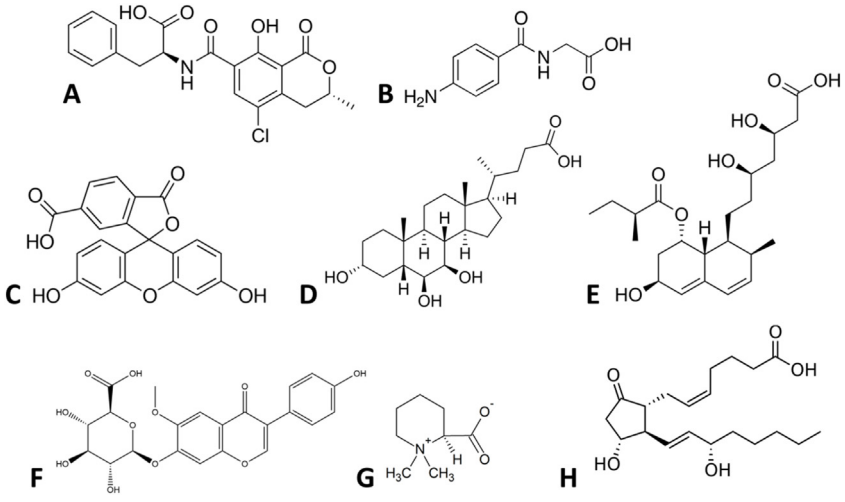

Fig. 3. Structure of molecules considered in the study. **A.** OTA. **B**. *para*-aminohippuric acid. **C.** 6-carboxyfluorescein. **D.** beta-muricholate. **E.** Pravastatin. **F.** Glycitein-7-glucuronide. **G.** Homostachydrine. **H.** Prostaglandin E2.

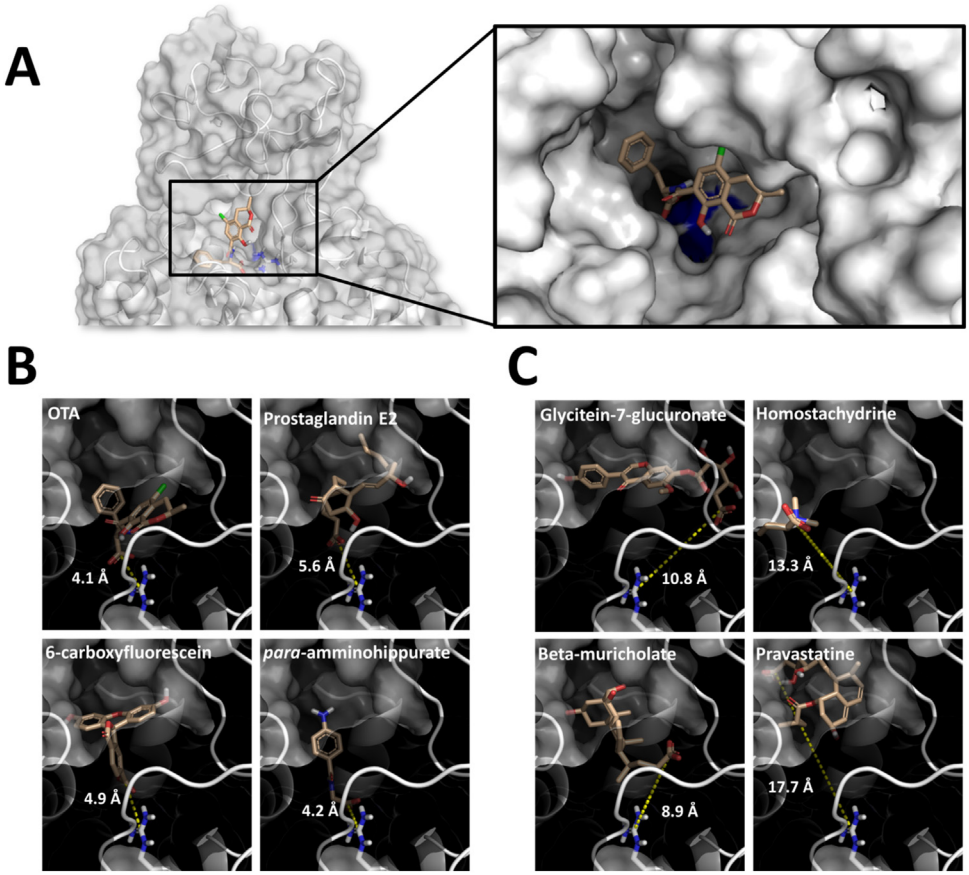

Fig. 4. Binding pose of substrates and decoys. The OAT1 is represented in semi-transparent surface and cartoon, while ligands are represented in sticks. Yellow dashed lines indicate the C-C distance between the carboxylic group of molecules and the guanidinium group of Arg134 (the distance is expressed in Å). **A.** Position and binding pose of OTA. In the close-up the capability of substrates to penetrate within the inner part of the surface cleft arranging the carboxylic group close to Arg134 (colored in blue) is exemplified. **B.** Binding architecture of substrates. **C.** Binding architecture of decoys.

3.2. Analysis of OAT1 variants

After the identification of the early mechanistic features to discriminate substrates from decoys, the 3D modeling approach was applied to a series of OAT1 mutated variants to assess whether mutations are expected to affect the mechanics underpinning the proper interaction of OTA as a substrate. The mutations considered in this study were found to occur in tumors, according to the BioMuta database (https://hive.biochemistry.gwu.edu/biomuta) that lists single-nucleotide variations occurring in cancer (Dingerdissen et al., 2018). Among the 164 mutations reported (last database access: 10th of May 2021), the mutations localized within 6 Å around the binding site were considered in this study as possibly directly involved in affecting the interaction with OTA. Specifically, 5 single-point mutations were found surrounding the OTA binding site and they were computed accordingly: S476R, R423P, D359N, Q361K, and E480K.

The effect of mutations on protein stability was assessed using the PremPS method (Chen et al., 2020), which accurately tests the effects of missense mutations on protein stability and estimates the unfolding Gibbs free energy changes ($\Delta\Delta G$). As shown in Table 1, four out of five mutations were found to have a theoretical limited effect on protein stability having $\Delta\Delta G < 1$ kcal/mol, in agreement with previous studies (Chen et al., 2020). For those, mutations were estimated to be compliant with actual expressions of the mutated proteins in cells. To note that S476R recorded a negative score (-0.56 kcal/mol) possibly pointing to a slight stabilising effect compared to the native protein. Conversely, R423 P recorded a score of 1.76 kcal/mol, suggesting a significant lower stability compared to the native protein. Its actual expression in cells was considered less probable compared to the other four proteins. Overall, all mutated residues were located at the solvent-exposed entrance of the OAT1 channel and these results were in line with previous evidence reporting substitutions of solvent-exposed residues with hydrophilic amino acids which do not impair generally protein stability (Reidhaarolson and Sauer, 1990; Strub et al., 2004). In addition, the substitution of solvent-exposed residues with arginine was found to improve the stability of a number of proteins (Strub et al., 2004). In this specific case, all mutated residues were hydrophilic and substituted in four out of five cases with hydrophilic residues, with a limited theoretical impact on the overall protein stability. Conversely, the R423P mutation may reasonably determine a reduced protein stability due to the lack of a hydrophilic side chain in a solvent-exposed region of the mutated variant.

In a next step, docking studies were performed on the mutated variants and docking scores did not allow to characterise whether mutations may prevent substrate recruitment of OTA by OAT1 since these all ranged between -8.0 and -7.5 kcal/mol. Therefore, the geometry of binding was inspected to investigate whether some of the mutations considered were expected to alter the substrate-like interaction between OTA and OAT1 described above. As shown in Fig. 6, four out of the five mutations considered in this study (R423 P, D359N, Q361K, and E480K) allowed an interaction of OTA similar to that with the wild type OAT1, having the carboxylic group sunk into the surface groove and close to the positively charged spot on its deepest inner part. Conversely, the substitution of Ser476 with Arg in the S476R variant resulted in a

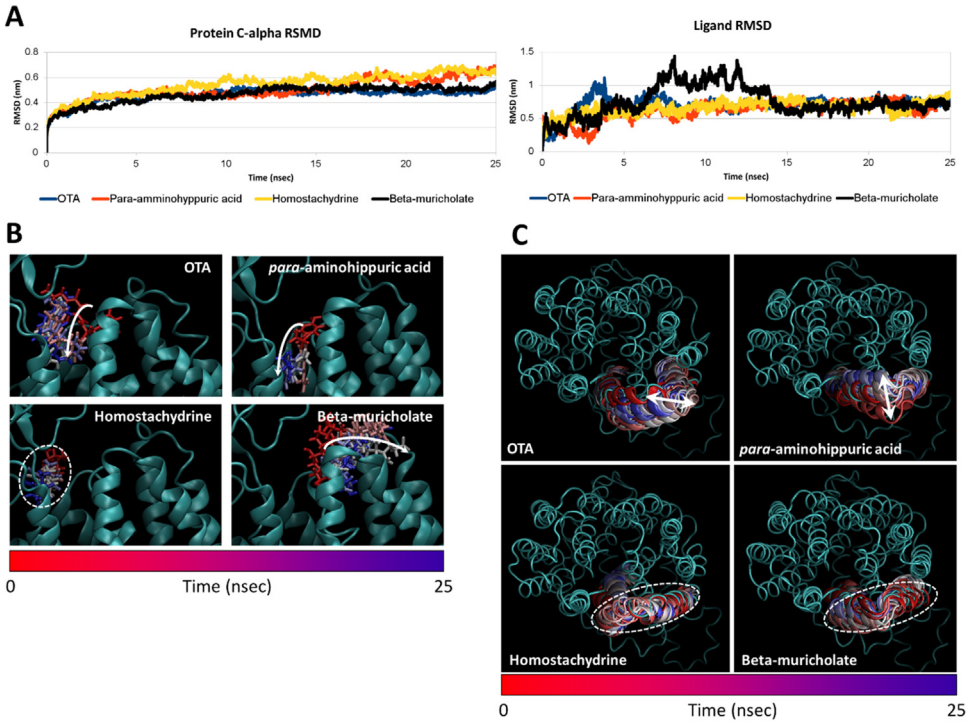

Fig. 5. Molecular dynamic results on wild type OAT1. **A.** Protein and ligands RMSD plots. **B.** Time-step representation of ligand trajectories. The ligands are represented in sticks while protein is represented in cartoon. The from-red-to-blue color switch indicates the stepwise changes of ligands coordinates along the simulation. The white arrows indicate the trajectory of ligands while the dashed white circle indicate the persistence of homostachydrine and the absence of appreciable inward or outward trajectories. **C.** Time-step representation of the induced-fit opening of the ligand binding site (helix 11 and 12) of OAT1 in complex with OTA, *para*-aminohippuric acid, beta-muricholate or homostachydrine. The from-red-to-blue color switch indicates the stepwise changes of coordinates along the simulation. The white arrows indicate the wide opening upon binding of OTA and *para*-aminohippuric acid, while white dashed circles indicate the very limited movements induced by beta-muricholate and homostachydrine.

Table 1
Estimate of the effects of mutation on the stability of OAT1.

Mutation	ΔΔG (kcal/mol)
S476R	−0.56
R423P	1.76
D359N	0.13
Q361K	0.35
E480K	0.6

re-shaping of the OTA binding site preventing the inclusion of its carboxylic group in the inner part of the binding site. Specifically, the carboxylic group of OTA was found arranged 10.9 Å away from the guanidinium group of Arg134 resembling the distance described for decoys (Table 2), compared to a value of 4.1 Å for the wild-type OAT1. On this basis, the OAT1 S476R variant in complex with OTA was further analyzed with molecular dynamic simulation to study possible effects of the mutation on the complex geometry and mechanics over the time. As shown in Fig. 6, the S476R mutation prevented the interaction with OTA as described for the wild type OAT1. Specifically, at the very beginning of the simulation OTA moved beneath its starting position, but then it stuck there being unable to trace the inward trajectory described for the wild type protein. In line with this observation, the opening of the upper part of the binding site was found much less wide than that observed in the wild type OAT1, suggesting a diminished tendency to let the substrate getting in as described above for OAT1 in complex with the two decoys. The S476R variant of OAT1 has been described in cancers from the oral cavity and may affect the capability of OAT1 to recruit OTA, and perhaps other OAT1 substrates, with potential consequences on the TK and TD in S476R-bearing individuals. Although the impairment of OTA recruitment in other OAT1 variants investigated here cannot be excluded, further studies investigating the impact of S476R variant on the TK and TD of OTA should be performed. The possible effects of OAT1 mutations on protein expression and stability in cells, as well as its *in vitro* transport activities should be further investigated to provide further insights on their potential effects

Table 2
Docking scores and C-C distance between ligand carboxylate and Arg143 guanidinium group.

Compound	Chemical type	Docking Score (kcal/mol)	Distance of COO^- from Arg134 (Å)
OTA	Substrate	−7.6	4.1
para-aminohippuric acid	Substrate	−5.4	4.2
6-carboxyfluorescein	Substrate	−8.3	4.9
Prostaglandin E2	Substrate	−5.3	5.6
Glycitein-7-glucuronate	Decoy	−8.2	10.8
Beta-muricholate	Decoy	−7.0	8.9
Homostachydrine	Decoy	−4.3	13.3
Pravastatin	Decoy	−6.4	17.7

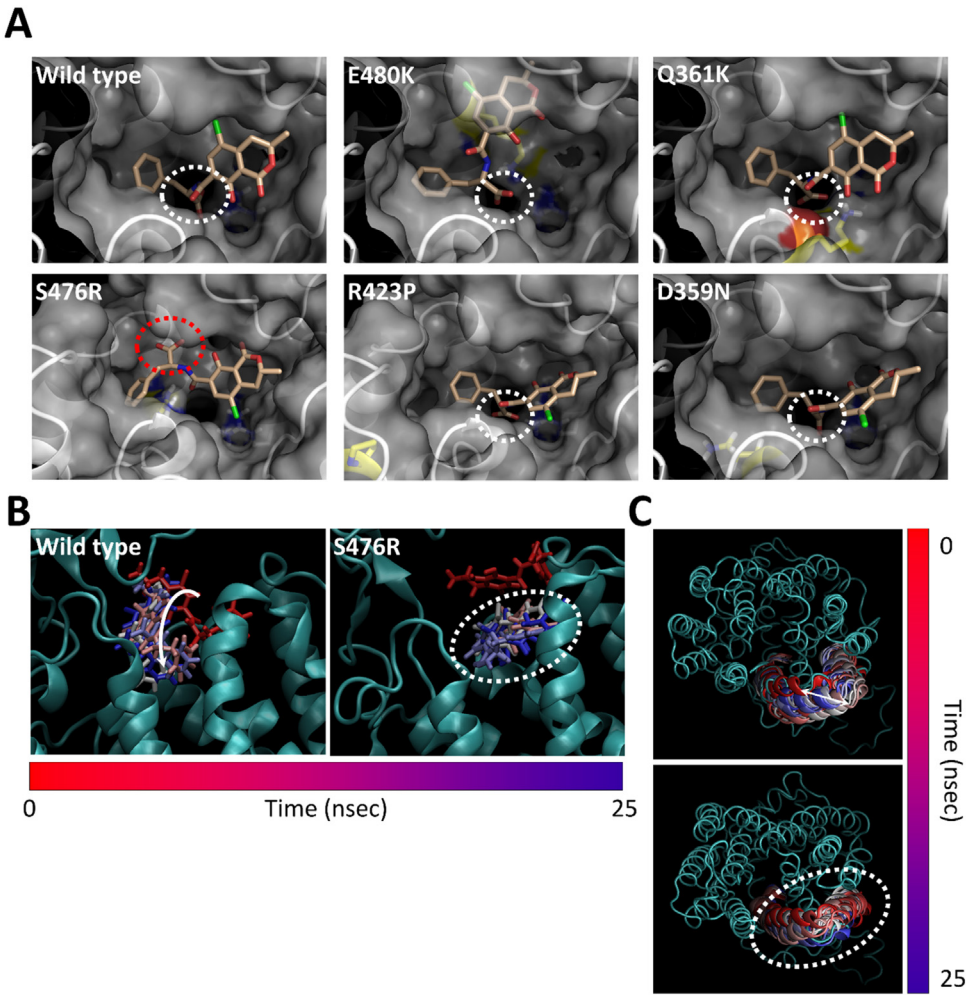

Fig. 6. Results of mutated OAT1 variants. **A.** Docking poses of OTA within the mutated variants of OAT1. Protein is represented in surface and cartoon, while OTA is represented in stick. Mutated residues are highlighted in yellow. White circles indicate the thrusting of carboxylate group into the inner part of surface cleft, while the red dashed circle indicates the improper arrangement of carboxylic acid outside the binding cleft in the S476R mutated variant. **B.** Time-step representation of OTA trajectories into wild type or S476R mutated variant of OAT1. OTA is represented in sticks while protein is represented in cartoon. The from-red-to-blue color switch indicates the stepwise changes of ligands coordinates along the simulation. The white arrow indicates the inward trajectory of OTA into the wild type OAT1. **C.** Comparison between the time-step representation of the induced-fit opening of the ligand binding site (helix 11 and 12) of the wild type or S476R mutated OAT1 in complex with OTA. The from-red-to-blue color switch indicates the stepwise changes of coordinates along the simulation.. The white arrow indicates the wide opening of the wild type OAT1, while the dashed white circle indicates the limited movements observed in its mutated version.

on human TK of OAT1 substrates, including OTA, and their related TD.

4. Conclusions and future applications

OAT1 is a key player in the excretion of various xenobiotics including OTA, a well-known mycotoxin relevant to the food safety area. The structural and molecular understanding of transporter proteins that play a role in xenobiotic excretion would support a kinetically informed risk assessment of their substrates. Furthermore, the development and application of informative and high throughput NAMs, including the one developed here, may provide useful non-testing approaches to support TK characterisation of a range of xenobiotics of relevance to food safety. Indeed, NAMs are meant to provide also a basis for a more informed mechanistic-based risk assessment (Lanzoni et al., 2019) and therefore the development of 3D models of proteins involved in toxicants' TK (like transporters and metabolising enzymes) may provide useful means to achieve that. So far, OAT1 has been poorly characterized from a structural and molecular standpoint, hampering mechanistically based kinetic analyses for its substrates. Over the years, only a few studies accounted for structural and molecular aspects of OAT1, mostly because of the challenge of developing 3D models of trans-membrane proteins when crystallographic or NMR data are scarce or unavailable. The present study took advantage of the very recent improvements of homology modeling techniques and updates of structural data recorded in PDB to develop an OAT1 3D model which allowed the identification of early structural and mechanistic features preluding the recruitment of OATs substrates to discriminate them from molecules that are not efficiently transported (i.e. decoys). It should be noted that the regulation of the trafficking machinery is a complex phenomenon (Okamoto, 2017) and the whole calculation of OAT1-mediated antiport of OTA, and related system biophysics are beyond the scope of this study and foreseen applications. Rather, this work aimed at identifying the very early molecular interaction events underpinning the OAT1-ligand complex formation, allowing the discrimination of substrates from decoys on the basis of the early capability of the formers to be recruited by OAT1. Keeping in mind that the model proposed does not account for all the dynamics of transport, uncertainties in the predictions can be expected. Specifically, the model is more likely prone to produce false positives, as molecules

providing a substrate-like interaction at the early stage, may abort the transport at later stages. Conversely, complexes that are computed during the timeframe considered as a) unstable and/or b) whit ligands tracing outward trajectories (like beta-muricholate) or having a stuck interaction at the transporter surface (like homostachydrine); are not likely to result in an efficient transport compared to those ligands demonstrating a fast entrance within the computed timeframe (like OTA and other probe substrates). Overall, these scenarios suggest a lower chance of false negative predictions and such a feature may prove useful in the context of a tiered approach particularly to select *in silico* transporter-substrate interactions for further investigation i.e. using *in vitro* transport studies to confirm or refute such *in silico* interactions. In this respect, the analysis of early mechanisms for OTA recruitment using short molecular dynamics, in terms of computational resources, warrants a fit for purpose pipeline and allows its potential straightforward extension to a broader set of chemicals, transporter proteins and/or mutated variants of interest. It should be noted that the workflow presented here relies on a fully open-source data sources fulfilling the current European demand to develop transparent and freely accessible methodologies to support a transparent and reproducible use of tools in risk assessment (Ingenbleek et al., 2021; Ioannidou et al., 2021). All the 3D structures of single molecules or OAT1 complexes generated in this work are freely available upon request.

Broadly speaking, such a pipeline also provides simulations of OTA interactions with transporters to investigate inter-species differences in the TK of OTA and the basis for setting safe exposure levels for humans based on animal toxicity data. Notwithstanding, differences in activity and/or expression of renal transporter proteins between species can play an important role in inter-species differences in TK. A recent study investigated differences in protein expression for a series of renal transporters between humans, monkeys (cynomolgus), dogs (beagle), rats (Wistar) and mice (CD-1) (Basit et al., 2019), including OAT1, OAT3 and OAT4. For OAT1, expression data for all species were included, whereas for OAT3 and OAT4, only expression data for humans and monkeys were included (lack of conserved peptides in other species). Reported expression of OAT3 and OAT4 is rather similar in cynomolgus monkeys and humans (i.e. slightly higher in monkeys), whereas larger differences in OAT1 expression are observed with a median protein abundance in the kidney of cynomolgus monkey > 2-fold higher compared to those in human kidney. Reported elimination phase half-lives ($t^1/_2\beta$) after oral exposure are available for humans and rhesus macaque, being 1.7-fold higher in humans compared to that in rhesus macaques (Dietrich et al., 2005). This suggests a possible role of differences in OAT1 expression in different elimination kinetics between these species. In addition, expression differences in cynomolgus monkeys vs rhesus macaques can be expected as well as differences in kinetic processes including different elimination half-lives, species-specific differences in plasma protein binding (Hagelberg et al., 1989), related glomerular filtration, and species-specific transporter activities. So far, there is little insight into species differences in transporter activities of OTA by OATs. To obtain such insights, studies with recombinant transporter proteins can be conducted as performed with human OAT1, OAT2 and OAT4 (Tsuda et al., 1999; Jung et al., 2001; Babu et al., 2002). The *in silico* approach presented here is expected to provide relevant insights in species differences in transporter activities and these can be compared to relevant *in vitro* findings and as a prediction tool. Overall, the pipeline presented here provides a scientific basis to assess early interactions between xenobiotics and transporter proteins as well as other xenobiotic-metabolising enzymes. Such mechanistic information on substrate recruitment and the impact of polymorphic variants can be used as part of a battery of NAMs and integrated with Michaelis-Menten kinetic *in vitro* data (Vmax, Km, etc.) for TK modeling. It is recommended to apply this framework to a range of isoform-specific probe substrates and relevant xenobiotics to food safety for which inter-individual differences in pharmacokinetics have been quantified. These include other transporters (P-gp, BCRP), Phase I enzymes such as Cytochrome P-450 [i.e. CYP1A2 (e.g. caffeine); CYP2D6 (e.g. metoprolol), CYP3A4 (e.g. midazolam), CYPC9 tolbutamide)] and phase II enzymes [e.g. UDP-glucuronyl-transferases (UGT) and glutathione-s-transferases (GST)] (Buratti et al., 2021; Darney et al., 2020; Kasteel et al., 2020; Quignot et al., 2021). Since a growing number of 3D structures are available for human xenobiotic-metabolising enzymes including some polymorphic variants, substrate recruitment can be compared across enzyme variants. A relevant example is the polymorphic variants for CYP2D6 which have been well characterised in Caucasian populations such as the CYP2D6*4 and the CYP2D6*10 phenotypes responsible for the poor metaboliser phenotype and a decreased enzyme function, respectively. The 3D molecular docking approach from the structured pipeline described here can be applied to investigate molecular descriptors of probe substrate recruitment for both polymorphic variants. In addition, since human variability in the kinetics of CYP2D6 probe substrates are available for probe substrates and polymorphic variants (e.g. metoprolol, desipramine, venlafaxine, fluoxetine, paroxetine, etc.), molecular descriptors of substrate recruitments can be compared and correlated with such differences in kinetics.

Such a non-testing *in silico* approach can open a new avenue to improve model development and implementation using mechanistic information and can ultimately allow the integration of inter-individual differences in the risk assessment process. These non-testing approaches are also promising to assess whether interspecies differences in metabolism and TK can be expected, which is critical when extrapolating animal data to humans for hazard characterisation. Such studies can provide structured lines of evidence relevant for risk assessment ranging from 1) the mechanistic basis of enzyme or transporter-ligand interaction in individuals with wild type and polymorphic phenotypes, 2) integration of pathway-related variability and *in vitro* metabolism data into quantitative *in vitro* to *in vivo* extrapolation (QIVIVE) models for relevant food xenobiotics, 3) integration of differences in TK (internal dose) from the QIVIVE and TD dose-response data using benchmark dose modeling to derive benchmark dose limits on an internal dose basis.

Declaration of Competing Interest

The authors declare the following financial interests/personal relationships which may be considered as potential competing interests:

Luca Dellafiora reports financial support was provided by European Food Safety Authority.

Acknowledgment

The work was carried out as part of the EFSA project “Data collection, update and further development of biologically-based models for humans and animal species to support transparency in food and feed safety” (OC/EFSA/SCER/2020/03).

Appendix A. Supplementary data

Supplementary material related to this article can be found, in the online version, at doi:https://doi.org/10.1016/j.toxlet.2021.11.001.

References

Abraham, M.J., Murtola, T., Schulz, R., Páll, S., Smith, J.C., Hess, B., Lindahl, E., 2015. GROMACS: high performance molecular simulations through multi-level parallelism from laptops to supercomputers. SoftwareX 1-2, 19–25.

Altschul, S.F., Madden, T.L., Schaffer, A.A., Zhang, J.H., Zhang, Z., Miller, W., Lipman, D. J., 1997. Gapped BLAST and PSI-BLAST: a new generation of protein database search programs. Nucleic. Acid Res. 25, 3389–3402.

Anzai, N., Jutabha, P., Endou, H., 2010. Molecular mechanism of ochratoxin a transport in the kidney. Toxins 2, 1381–1398.

Babu, E., Takeda, M., Narikawa, S., Kobayashi, Y., Enomoto, A., Tojo, A., Cha, S.H., Sekine, T., Sakthisekaran, D., Endou, H., 2002. Role of human organic anion transporter 4 in the transport of ochratoxin A. Biochimica Et Biophysica Acta-Molecular Cell Research 1590, 64–75.

Bateman, A., Martin, M.J., Orchard, S., Magrane, M., Agivetova, R., Ahmad, S., Alpi, E., Bowler-Barnett, E.H., Britto, R., Bursteinas, B., Bye-A-Jee, H., Coetzee, R., Cukura, A., Da Silva, A., Denny, P., Dogan, T., Ebenezer, T., Fan, J., Castro, L.G., Garmiri, P., Georghiou, G., Gonzales, L., Hatton-Ellis, E., Hussein, A., Ignatchenko, A., Insana, G., Ishtiaq, R., Jokinen, P., Joshi, V., Jyothi, D., Lock, A., Lopez, R., Luciani, A., Luo, J., Lussi, Y., Mac-Dougall, A., Madeira, F., Mahmoudy, M., Menchi, M., Mishra, A., Moulang, K., Nightingale, A., Oliveira, C.S., Pundir, S., Qi, G.Y., Raj, S., Rice, D., Lopez, M.R., Saidi, R., Sampson, J., Sawford, T., Speretta, E., Turner, E., Tyagi, N., Vasudev, P., Volynkin, V., Warner, K., Watkins, X., Zaru, R., Zellner, H., Bridge, A., Poux, S., Redaschi, N., Aimo, L., Argoud-Puy, G., Auchincloss, A., Axelsen, K., Bansal, P., Baratin, D., Blatter, M.C., Bolleman, J., Boutet, E., Breuza, L., Casals-Casas, C., de Castro, E., Echioukh, K.C., Coudert, E., Cuche, B., Doche, M., Dornevil, D., Estreicher, A., Famiglietti, M.L., Feuermann, M., Gasteiger, E., Gehant, S., Gerritsen, V., Gos, A., Gruaz-Gumowski, N., Hinz, U., Hulo, C., Hyka-Nouspikel, N., Jungo, F., Keller, G., Kerhornou, A., Lara, V., Le Mercier, P., Lieberherr, D., Lombardot, T., Martin, X., Masson, P., Morgat, A., Neto, T.B., Paesano, S., Pedruzzi, I., Pilbout, S., Pourcel, L., Pozzato, M., Pruess, M., Rivoire, C., Sigrist, C., Sonesson, K., Stutz, A., Sundaram, S., Tognolli, M., Verbregue, L., Wu, C.H., Arighi, C.N., Arminski, L., Chen, C.M., Chen, Y.X., Garavelli, J.S., Huang, H.Z., Laiho, K., McGarvey, P., Natale, D.A., Ross, K., Vinayaka, C.R., Wang, Q.H., Wang, Y.Q., Yeh, L.S., Zhang, J., UniProt, C., 2021. UniProt: the universal protein knowledgebase in 2021. Nucleic Acid Res 49, D480–D489.

Berman, H.M., Westbrook, J., Feng, Z., Gilliland, G., Bhat, T.N., Weissig, H., Shindyalov, I.N., Bourne, P.E., 2000. The protein data bank. Nucleic. Acid. Res. 28, 235–242.

Best, R.B., Zhu, X., Shim, J., Lopes, P.E., Mittal, J., Feig, M., Mackerell, A.D.J., 2012. Optimization of the additive CHARMM all-atom protein force field targeting improved sampling of the backbone φ, ψ and side-chain $\chi(1)$ and $\chi(2)$ dihedral angles. J. Chem. Theory Comput. 8, 3257–3273.

Buratti, F.M., Darney, K., Vichi, S., Turco, L., Di Consiglio, E., Lautz, L.S., Bechaux, C., Dorne, J., Testai, E., 2021. Human variability in glutathione-S-transferase activities, tissue distribution and major polymorphic variants: meta-analysis and implication for chemical risk assessment. Toxicol. Lett. 337, 78–90.

Bush, K.T., Wu, W., Lun, C., Nigam, S.K., 2017. The drug transporter OAT3 (SLC22A8) and endogenous metabolite communication via the gut-liver-kidney axis. J. Biol. Chem. 292, 15789–15803.

Buxhofer-Ausch, V., Nemet, O., Sheikh, M., Andrikovics, H., Reiner, A., Ausch, C., Mechtcheriakova, D., Tordai, A., Gleiss, A., Ozvegy-Laczka, C., Jager, W., Thalhammer, T., 2020. Two common polymorphic variants of OATP4A1 as potential risk factors for colorectal cancer. Oncol. Lett. 20.

Chen, Y.T., Lu, H.Y., Zhang, N., Zhu, Z.F., Wang, S.Q., Li, M.H., 2020. PremPS: predicting the impact of missense mutations on protein stability. PLoS Comput. Biol. 16.

Cihlar, T., Ho, E.S., 2000. Fluorescence-based assay for the interaction of small molecules with the human renal organic anion transporter 1. Anal. Biochem. 283, 49–55.

Clerbaux, L.A., Paini, A., Lumen, A., Osman-Ponchet, H., Worth, A.P., Fardel, O., 2019. Membrane transporter data to support kinetically-informed chemical risk assessment using non-animal methods: scientific and regulatory perspectives. Environ. Int. 126, 659–671.

Darney, K., Turco, L., Buratti, F.M., Di Consiglio, E., Vichi, S., Roudot, A.C., Bechaux, C., Testai, E., Dorne, J., Lautz, L.S., 2020. Human variability in influx and efflux transporters in relation to uncertainty factors for chemical risk assessment. Food Chem. Toxicol. 140.

Dellafiora, L., Galaverna, G., Dall'Asta, C., Cozzini, P., 2015. Hazard identification of cis/trans-zearalenone through the looking-glass. Food Chem. Toxicol. 86, 65–71.

Deng, D., Xu, C., Sun, P.C., Wu, J.P., Yan, C.Y., Hu, M.X., Yan, N., 2014. Crystal structure of the human glucose transporter GLUT1. Nature 510, 121-+..

Dietrich, D.R., Heussner, A.H., O'Brien, E., 2005. Ochratoxin A: comparative pharmacokinetics and toxicological implications (experimental and domestic animals and humans). Food Addit Contam A 22, 45–52.

Dingerdissen, H.M., Torcivia-Rodriguez, J., Hu, Y., Chang, T.C., Mazumder, R., Kahsay, R., 2018. BioMuta and BioXpress: mutation and expression knowledgebases for cancer biomarker discovery. Nucleic Acid Res 46, D1128–D1136.

EFSA, 2020. Risk assessment of ochratoxin A in food. EFSA J. 18, e06113.

El-Sheikh, A.A.K., Masereeuw, R., Russel, F.G.M., 2008. Mechanisms of renal anionic drug transport. Eur. J. Pharmacol. 585, 245–255.

Fujita, T., Brown, C., Carlson, E.J., Taylor, T., de la Cruz, M., Johns, S.J., Stryke, D., Kawamoto, M., Fujita, K., Castro, R., Chen, C.W., Lin, E.T., Brett, C.M., Burchard, E. G., Ferrin, T.E., Huang, C.C., Leabman, M.K., Giacomini, K.M., 2005. Functional analysis of polymorphisms in the organic anion transporter, SLC22A6 (OAT1). Pharmacogenet. Genomics 15, 201–209.

Graves, A.P., Brenk, R., Shoichet, B.K., 2005. Decoys for docking. J. Med. Chem. 48, 3714–3728.

Hagelberg, S., Hult, K., Fuchs, R., 1989. Toxicokinetics of OCHRATOXIN-A in several species and its PLASMA-BINDING Properties. J. Appl. Toxicol. 9, 91–96.

Ingenbleek, L., Lautz, L.S., Dervilly, G., Darney, K., Astuto, M.C., Tarazona, J., Liem, A.K. D., Kass, G.E.N., Leblanc, J.C., Verger, P., Le Bizec, B., Dorne, J.L.C.M., 2021. Risk assessment of chemicals in food and feed: principles, applications and future perspectives. Environ. Pollut. Exposures Public Health Royal Soc. Chem. 1–38.

Ioannidou, S., Cascio, C., Gilsenan, M.B., 2021. European Food Safety Authority open access tools to estimate dietary exposure to food chemicals. Environ. Int. 149.

Islinger, F., Gekle, M., Wright, S.H., 2001. Interaction of 2,3-dimercapto-1-propane sulfonate with the human organic anion transporter hOAT1. J. Pharmacol. Exp. Ther. 299, 741–747.

Jung, K.Y., Takeda, M., Kim, D.K., Tojo, A., Narikawa, S., Yoo, B.S., Hosoyamada, M., Cha, S.H., Sekine, T., Endou, H., 2001. Characterization of ochratoxin A transport by human organic anion transporters. Life Sci. 69, 2123–2135.

Kapoor, K., Finer-Moore, J.S., Pedersen, B.P., Caboni, L., Waight, A., Hillig, R.C., Bringmann, P., Heisler, I., Muller, T., Siebeneicher, H., Stroud, R.M., 2016. Mechanism of inhibition of human glucose transporter GLUT1 is conserved between cytochalasin B and phenylalanine amides. Proc. Natl. Acad. Sci. U. S. A. 113, 4711–4716.

Kasteel, E.E.J., Darney, K., Kramer, N.I., Dorne, J., Lautz, L.S., 2020. Human variability in isoform-specific UDP-glucuronosyltransferases: markers of acute and chronic exposure, polymorphisms and uncertainty factors. Arch. Toxicol. 94, 2637–2661.

Kim, S., Chen, J., Cheng, T.J., Gindulyte, A., He, J., He, S.Q., Li, Q.L., Shoemaker, B.A., Thiessen, P.A., Yu, B., Zaslavsky, L., Zhang, J., Bolton, E.E., 2021. PubChem in 2021: new data content and improved web interfaces. Nucleic Acid Res. 49, D1388–D1395.

Kimura, H., Takeda, M., Narikawa, S., Enomoto, A., Ichida, K., Endou, H., 2002. Human organic anion transporters and human organic cation transporters mediate renal transport of prostaglandins. J. Pharmacol. Exp. Ther. 301, 293–298.

Lai, R.E., Jay, C.E., Sweet, D.H., 2018. Organic solute carrier 22 (SLC22) family: potential for interactions with food, herbal/dietary supplements, endogenous compounds, and drugs. J. Food Drug Anal. 26, S45–S60.

Lanzoni, A., Castoldi, A.F., Kass, G.E.N., Terron, A., De Seze, G., Bal-Price, A., Bois, F.Y., Delclos, K.B., Doerge, D.R., Fritsche, E., Halldorsson, T., Kolossa-Gehring, M., Hougaard Bennekou, S., Koning, F., Lampen, A., Leist, M., Mantus, E., Rousselle, C., Siegrist, M., Steinberg, P., Tritscher, A., Van de Water, B., Vineis, P., Walker, N., Wallace, H., Whelan, M., Younes, M., 2019. Advancing human health risk assessment. EFSA J. 17 (S1) e170712 21 pp. 2019.

Larkin, M.A., Blackshields, G., Brown, N.P., Chenna, R., McGettigan, P.A., McWilliam, H., Valentin, F., Wallace, I.M., Wilm, A., Lopez, R., Thompson, J.D., Gibson, T.J., Higgins, D.G., 2007. Clustal W and clustal X version 2.0. Bioinformatics 23, 2947–2948.

Mirdita, M., von den Driesch, L., Galiez, C., Martin, M.J., Soding, J., Steinegger, M., 2017. Uniclust databases of clustered and deeply annotated protein sequences and alignments. Nucleic Acid Res. 45, D170–D176.

Morrissey, K.M., Wen, C.C., Johns, S.J., Zhang, L., Huang, S.M., Giacomini, K.M., 2012. The UCSF-FDA TransPortal: a public drug transporter database. Clin. Pharmacol. Ther. 92, 545–546.

Ng, C.A., Hungerbuehler, K., 2015. Exploring the use of molecular docking to identify bioaccumulative perfluorinated alkyl acids (PFAAs). Environ. Sci. Technol. 49, 12306–12314.

Nigam, S.K., Bush, K.T., Martovetsky, G., Ahn, S.Y., Liu, H.C., Richard, E., Bhatnagar, V., Wu, W., 2015. The organic anion transporter (OAT) family: a SYSTEMS BIOLOGY PERSPECTIVE. Physiol. Rev. 95, 83–123.

Okamoto, C.T., 2017. Regulation of transporters and channels by membrane-trafficking complexes in epithelial cells. Cold Spring Harb. Perspect. Biol. 9.

Paulsen, P.A., Custodio, T.F., Pedersen, B.P., 2019. Crystal structure of the plant symporter STP10 illuminates sugar uptake mechanism in monosaccharide transporter superfamily. Nat. Commun. 10.

Pelis, R.M., Wright, S.H., 2014. SLC22, SLC44, and SLC47 transporters-organic anion and cation transporters: molecular and cellular properties. In: Bevensee, M.O. (Ed.), Exchangers, vol. 73. , pp. 233–261.

Pettersen, E.F., Goddard, T.D., Huang, C.C., Couch, G.S., Greenblatt, D.M., Meng, E.C., Ferrin, T.E., 2004. UCSF chimera - A visualization system for exploratory research and analysis. J. Comput. Chem. 25, 1605–1612.

Pickova, D., Ostry, V., Malir, J., Toman, J., Malir, F., 2020. A review on mycotoxins and Microfungi in spices in the light of the last five years. Toxins 12.

Quignot, N., Wiecek, W., Lautz, L., Dorne, J.L., Amzal, B., 2021. Inter-phenotypic differences in CYP2C9 and CYP2C19 metabolism: bayesian meta-regression of human population variability in kinetics and application in chemical risk assessment. Toxicol. Lett. 337, 111–120.

Reidhaarolson, J.F., Sauer, R.T., 1990. Functionally acceptable substitutions in 2 aLPHA-hELICAL regions of Lambda repressor. Proteins-Structure Function Genetics 7, 306–316.

Ringot, D., Chango, A., Schneider, Y.J., Larondelle, Y., 2006. Toxicokinetics and toxicodynamics of ochratoxin A, an update. Chem. Biol. Interact. 159, 18–46.

Rocha, K.C., Pereira, B.M.V., Rodrigues, A.C., 2018. An update on efflux and uptake transporters as determinants of statin response. Expert Opin. Drug Metab. Toxicol. 14, 613–624.

Saito, H., 2010. Pathophysiological regulation of renal SLC22A organic ion transporters in acute kidney injury: pharmacological and toxicological implications. Pharmacol. Ther. 125, 79–91.

Simons, K.T., Bonneau, R., Ruczinski, I., Baker, D., 1999. Ab initio protein structure prediction of CASP III targets using ROSETTA. Proteins-Structure Function Bioinformatics 171–176.

Sissung, T.M., Goey, A.K.L., Ley, A.M., Strope, J.D., Figg, W.D., 2014. Pharmacogenetics of membrane transporters: a review of current approaches, 2nd edition In: Yan, Q. (Ed.), Pharmacogenomics in Drug Discovery and Development, 1175. , pp. 91–120.

Strub, C., Alies, C., Lougarre, A., Ladurantie, C., Czaplicki, J., Fournier, D., 2004. Mutation of exposed hydrophobic amino acids to arginine to increase protein stability. BMC Biochem. 5.

Sweet, D.H., 2005. Organic anion transporter (Slc22a) family members as mediators of toxicity. Toxicol. Appl. Pharmacol. 204, 198–215.

Takeda, M., Noshiro, R., Onozato, M.L., Tojo, A., Hasannejad, H., Huang, X.L., Narikawa, S., Endou, H., 2004. Evidence for a role of human organic anion transporters in the muscular side effects of HMG-CoA-reductase inhibitors. Eur. J. Pharmacol. 483, 133–138.

Trott, O., Olson, A.J., 2010. AutoDock Vina: improving the speed and accuracy of docking with a new scoring function, efficient optimization, and multithreading. J. Comput. Chem. 31, 455–461.

Tsuda, M., Sekine, T., Takeda, M., Cha, S.H., Kanai, Y., Kimura, M., Endou, H., 1999. Transport of ochratoxin A by renal multispecific organic anion transporter 1. J. Pharmacol. Exp. Ther. 289, 1301–1305.

Wang, Z., Cui, T., Ci, X.Y., Zhao, F., Sun, Y.H., Li, Y.Z., Liu, R., Wu, W.D., Yi, X.L., Liu, C.X., 2019. The effect of polymorphism of uric acid transporters on uric acid transport. J. Nephrol. 32, 177–187.

Williams, A.J., Lambert, J.C., Thayer, K., Dorne, J., 2021. Sourcing data on chemical properties and hazard data from the US-EPA CompTox Chemicals Dashboard: a practical guide for human risk assessment. Environ. Int. 154.

Wong, C.C., Botting, N.P., Orfila, C., Al-Maharik, N., Williamson, G., 2011. Flavonoid conjugates interact with organic anion transporters (OATs) and attenuate cytotoxicity of adefovir mediated by organic anion transporter 1 (OAT1/SLC22A6). Biochem. Pharmacol. 81, 942–949.

Xu, L., Chen, L.Y., 2020. Molecular determinant of substrate binding and specificity of cytochrome P450 2J2. Sci. Rep. 10.

Yang, J.Y., Anishchenko, I., Park, H., Peng, Z.L., Ovchinnikov, S., Baker, D., 2020. Improved protein structure prediction using predicted interresidue orientations. Proc. Natl. Acad. Sci. U. S. A. 117, 1496–1503.

Zhang, Y., Skolnick, J., 2004. Scoring function for automated assessment of protein structure template quality. Proteins-Structure Function Bioinformatics 57, 702–710.

Zhang, J.H., Wang, H.X., Fan, Y.Z., Yu, Z., You, G.F., 2021. Regulation of organic anion transporters: role in physiology, pathophysiology, and drug elimination. Pharmacol. Ther. 217.

Zoete, V., Cuendet, M.A., Grosdidier, A., Michielin, O., 2011. SwissParam: a fast force field generation tool for small organic molecules. J. Comput. Chem. 32, 2359–2368.